Journal of Solid State Chemistry 184 (2011) 357–364

Contents lists available at ScienceDirect

Journal of Solid State Chemistry

journal homepage: www.elsevier.com/locate/jssc

$CdWO_4$ polymorphs: Selective preparation, electronic structures, and photocatalytic activities

Tingjiang Yan, Liping Li, Wenming Tong, Jing Zheng, Yunjian Wang, Guangshe Li *

State Key Laboratory of Structural Chemistry, Fujian Institute of Research on the Structure of Matter, Graduate School of Chinese Academy of Sciences, Fuzhou 350002, People's Republic of China

ARTICLE INFO

Article history:
Received 4 September 2010
Received in revised form
2 December 2010
Accepted 7 December 2010
Available online 14 December 2010

Keywords:
$CdWO_4$
Polymorphs
Electronic structure
Photocatalytic activity

ABSTRACT

This work explored the selective synthesis of polymorphs of $CdWO_4$ in either tetragonal or monoclinic phase by optimizing the experimental parameters. Systematic characterization indicated that both polymorphs possessed similar spherical morphologies but different structural building blocks. Electronic structures calculations for both polymorphs demonstrated the same constructions of conduction band or valence band, while the conduction band widths of both polymorphs were quite different. Both $CdWO_4$ polymorphs exhibited good photocatalytic activity for degradation of methyl orange under UV light irradiation. When comparing to some other well-known tungstate oxide materials, the photocatalytic activity was found to follow such a consequence, monoclinic $CdWO_4 \approx$ monoclinic $ZnWO_4 >$ tetragonal $CdWO_4 >$ tetragonal $CaWO_4$. The specific photocatalytic activity of monoclinic $CdWO_4$ was even higher than that of commercial TiO_2 photocatalyst (Degussa P25). The increased activity from the tetragonal $CdWO_4$ to the monoclinic was consistent with the trend of the decreased symmetry, and this could be explained in terms of the geometric structures and electronic structures for both polymorphs.

1. Introduction

Semiconductors have many highly structurally sensitive properties that are necessary for technological applications, among which photocatalytic oxidation becomes one of the promising routes for environmental remediation [1–7]. It is well established that many organic and inorganic pollutants existing in waste water can be completely decomposed by photocatalysis. As a well-known semiconductor, TiO_2 is proven to show photocatalytic activity for oxidative decomposition of organic compounds [1–3]. Nevertheless, TiO_2 is featured by both inherent slow reaction rate and poor solar efficiency that have hindered its further applications [8,9]. Several structural modification techniques like doping have been devoted to improving the photocatalytic performance, while the activity of TiO_2 is rather limited [10–12]. Recently, some alternative oxide materials like tantalites [4,13], vanadates [14,15], molybdates [16], niobates [17,18], and tungstates [19–24] have been investigated to obtain high photocatalytic activity for water splitting or/and organic pollutants degradation. In spite of some progresses, stably achieving highly photocatalytic activity in the mixed oxide semiconductors still remains a great challenge.

The basis of searching for effective photocatalysts is the understanding of the nature of photocatalysis and its relevant influencing factors. It is documented that the activity of a photocatalyst is closely related to surface area, morphology, crystal structure, and electronic structure as well. The surface area and morphology can be taken as external factors since they can be well controlled by experimental conditions, while crystal structure and electronic structure are intrinsic nature of the photocatalytic activities. Concerning the impacts of crystal structure, Hou et al. [25] developed three Ga_2O_3 polymorphs and found that the structural type was a great concern to the photocatalytic activities. Nevertheless, the contribution of the electronic structures to the photocatalytic properties of Ga_2O_3 polymorphs is not clear. Indeed, from the viewpoints of materials chemistry and physical chemistry, crystal structure directly determines the electronic structure and furthermore the photocatalytic properties. Tang and Ye [26] theoretically investigated the photocatalytic properties of three tungstate oxides ($Bi_2W_2O_9$, Ag_2WO_4, and $AgBiW_2O_8$) on the basis of the electronic structures, while these target materials have different structural types or chemical compositions that complicate the photocatalytic mechanism. Ouyang et al. [27] studied the correlation of crystal structures, electronic structures, and photocatalytic property by studying a series of Ag-based oxides ($AgAlO_2$, $AgCrO_2$, and Ag_2CrO_4). But still, the different chemical composition and crystal structural types as well as energy band structures make it very difficult to figure out the nature of the photocatalysis. Therefore, selecting a semiconductor of polymorphs as the target and studying the impacts of crystal structure and electronic structure on the photocatalytic property are pivotal to gain the insights into the photocatalytic mechanism that is highly useful for exploring novel photocatalytic materials.

$CdWO_4$ is a typical polymorphic semiconductor that finds broad applications in optical, electronic, and catalytic fields [28–34]. Due

* Corresponding author. Fax: +86 591 83702122.
E-mail address: guangshe@fjirsm.ac.cn (G. Li).

0022-4596/$ - see front matter © 2010 Elsevier Inc. All rights reserved.
doi:10.1016/j.jssc.2010.12.013

to its low radiation damage, high average refractive index, and high X-ray absorption coefficient, $CdWO_4$ has been widely used as a popular X-ray scintillator [28] and an advanced medical X-ray detector in computerized tomography [29]. The band-gap for $CdWO_4$ is as broad as 3.8 eV, which is much larger than 3.2 eV for TiO_2 and thus seems to indicate that the photo-absorption can only be limited to the wavelengths shorter than that of TiO_2. Nevertheless, it is well established that the broader band-gap is highly probable to give larger redox ability that allows great photocatalytic performance. Therefore, $CdWO_4$ represents an example of a potential highly efficient photocatalytic material. Up to now, very limited investigations have confirmed that the photocatalytic activity for the monoclinic $CdWO_4$ is comparable with the well-known TiO_2 [34], though the impacts of the polymorphs on the photocatalytic performance are still unknown. $CdWO_4$ has two polymorphs: monoclinic wolframite structure and tetragonal scheelite structure depending on the preparation conditions. Generally, the former one is thermodynamically stable at room temperature and can be easily prepared [35–41], whereas the latter one is metastable which could only be achieved under an extremely high pressure above 20 GPa [42]. A recent preparation work [43] on tetragonal $CdWO_4$ by simple solvothermal conditions raises the hope of understanding the impacts of the polymorphs on the photocatalytic performance of $CdWO_4$, while there is still lack of effective control over the polymorphs of $CdWO_4$.

In this work, two polymorphs of $CdWO_4$ in tetragonal or monoclinic form were selectively prepared from an aqueous solvothermal process by simply optimizing the reaction parameters. Photocatalytic properties were evaluated by degradation of MO dye in aqueous solutions under UV light irradiation. Based on the physicochemical properties and the electronic structures, the influences of crystal structures and electronic structures on the photocatalytic activities of $CdWO_4$ were systematically investigated.

2. Experimental section

2.1. Sample preparation

$CdWO_4$ polymorphs were synthesized by aqueous solvothermal processes. All chemicals were analytical grade, used without further purification. The synthetic procedures for the samples are described as follows:

Monoclinic $CdWO_4$ Appropriate amounts of $Na_2WO_4 \cdot 2H_2O$ and $CdCl_2 \cdot 2.5H_2O$ were put into a 100-mL stainless steel autoclave, and then 80 mL of distilled water was added with strongly magnetic stirring at room temperature. The autoclave was allowed to be heated at 200 °C for 10 h, then air cooled to room temperature. The resulting precipitates were collected and washed with distilled water and anhydrous ethanol for several times separately, and finally dried at 80 °C in air. For comparison, monoclinic $ZnWO_4$ and tetragonal $CaWO_4$ were also prepared according to this hydrothermal method.

Tetragonal $CdWO_4$ Appropriate amounts of $CdCl_2 \cdot 2.5H_2O$ and $Na_2WO_4 \cdot 2H_2O$ were separately dissolved in distilled water and then mixed together to form a homogeneous precipitate. The fresh precipitate was sufficiently washed with anhydrous ethanol and transferred to propylene glycol, which was sealed in autoclave and maintained at 200 °C for 10 h. The cooled precipitates were collected and washed, respectively, with distilled water and anhydrous ethanol for several times, and finally dried at 80 °C in air.

2.2. Characterizations

X-ray diffraction (XRD) patterns of the samples were collected on a Rigaku 2000 apparatus with Cu $K\alpha$ irradiation. Lattice parameters and atomic positions were calculated using Retica Rietveld program with peak positions that are calibrated by internal standard of nickel. Electronic structures of the samples were calculated based on plane wave density functional theory (DFT) using CASTEP program [44]. All band structures and density of states were calculated on the corresponding optimized crystal geometries. Raman spectra of the samples were recorded using a Perkin-Elmer Spectrum 2000R NIR FT-Raman spectrophotometer, equipped with a Nd/YAG laser and a InGaAs detector. The specific surface areas of the samples were determined from the nitrogen adsorption data at liquid nitrogen temperature using the Barrett–Emmett–Teller (BET) technique on a Micromeritics ASAP 2000 surface area and porosity analyzer. A Varian Cary 500 Scan UV/Vis system was used to obtain the optical absorption spectra of the samples over a range of 200–800 nm. The morphologies and microstructures of the samples were investigated by scanning electron microscopy (SEM) on a JSM6700F apparatus working at 10 kV. The photoluminescence (PL) spectra were measured using an Edinburgh Analytical Instruments FL/FSTCSPC920 fluorescence spectrophotometer.

2.3. Photocatalytic activities

Photocatalytic experiments were performed in a quartz tube with 4.6 cm inner diameter and 17 cm length. Four 4 W UV lamps with a wavelength centered at 254 nm (Philips, TUV 4W/G4 T5) were used as illuminating source. In a typical experiment, 150 mg of $CdWO_4$ photocatalysts were suspended in 150 mL aqueous solutions containing 10 ppm methyl orange (MO). Prior to irradiation, the suspension was magnetically stirred in the dark to ensure establishment of an adsorption/desorption equilibrium. During irradiation, 3 mL aliquots were sampled at the given time intervals and centrifuged to remove the catalysts. The filtrates were analyzed on a Perkin-Elmer UV WinLab Lambda 35 spectrophotometer. The percentage of degradation is reported as C/C_0, where C was the main absorption peak intensity of MO at each irradiated time interval at wavelength of 464 nm and C_0 was the absorption intensity of starting concentration of MO. The Cd^{2+} content in the residual solution after photocatalytic degradation was determined using Ultima2 inductively coupled plasma (ICP) spectrometry.

3. Results and discussion

3.1. Optimum condition for the selective formation of tetragonal and monoclinic $CdWO_4$ phases

Selective formation of tetragonal $CdWO_4$ phase was studied by optimizing two important parameters of the preparation conditions: the starting materials and solvents. First, the starting materials were kept the same as $CdCl_2 \cdot 2.5H_2O$ and $Na_2WO_4 \cdot 2H_2O$, while the solvent was adjusted for all preparations. When using water as the solvent, as indicated by XRD in Fig. 1a, the product was a pure monoclinic phase, which is characterized by diffraction peaks at 2θ of 23.28°, 29.00°, 29.55°, 30.51°, 35.37°, 35.68°, 47.65°, and 50.76° that match well the standard data for the monoclinic $CdWO_4$ (JCPDS, No. 14-0676). All diffraction peaks are sharp and intense, which demonstrate the high crystallinity. When water solvent was partially replaced by propylene glycol, the product still remained in the monoclinic phase, while all diffraction peaks became broadened (Fig. 1b). Therefore, addition of propylene glycol in the reaction systems reduced the particle size of the final monoclinic $CdWO_4$.

Further, when water solvent was completely replaced by propylene glycol, the product was a mixed phase of monoclinic

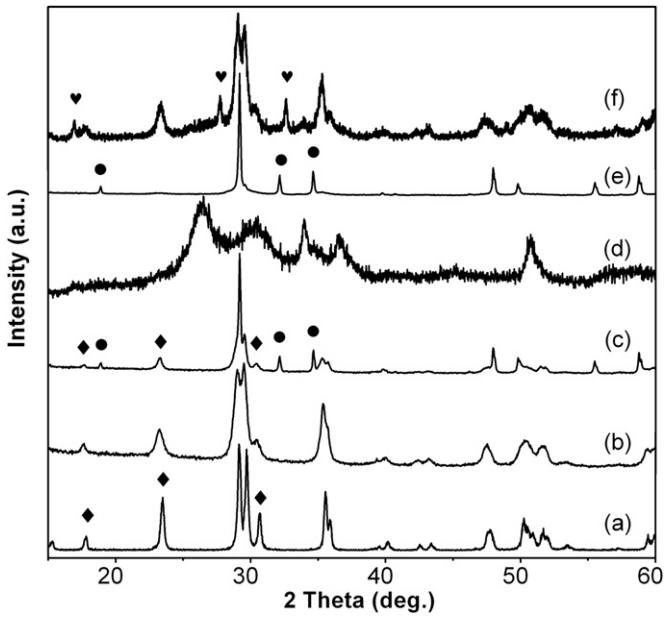

Fig. 1. XRD patterns of the samples synthesized under different conditions using the same starting materials $CdCl_2 \cdot 2.5H_2O$ and $Na_2WO_4 \cdot 2H_2O$ but with different solvents of (a) water, (b) mixture of water and propylene glycol, and (c) propylene glycol; and XRD patterns of (d) the precursor obtained in the first step; (e) the sample obtained using the precursor as starting material with a solvent of propylene glycol; and (f) the sample obtained using anhydrous metal salts as the starting materials. Symbols ● and ♦ represent the tetragonal and monoclinic $CdWO_4$, respectively, while ♥ denotes the unknown reflection peaks.

and tetragonal (Fig. 1c), different from the pure tetragonal $CdWO_4$ as reported by Rondinone et al. [43] using similar solvent. As well known, in a solvothermal or hydrothermal reaction system, the saturated vapor pressure, which is derived from the loaded solutions volume, is crucial to the formation of the final crystal phase. In this case, we can speculate that the different loaded volume of propylene glycol (80 mL vs 40 mL) between our and Rondinone et al. [43] might account for the different products. From Fig. 1c, it is also seen that the diffraction intensity for the tetragonal is much weaker than those for the monoclinic. Simply varying the types of the solvents such as from propylene glycol to ethylene glycol cannot lead to the formation of single-phase tetragonal $CdWO_4$ because of the progressive formation of the monoclinic component [43,45]. This observation may explain the bare reports [43] in literature for the tetragonal $CdWO_4$, since tetragonal $CdWO_4$ is thermodynamically metastable and would readily convert into the monoclinic at high temperatures (see below).

These results have dual important implications: (1) addition of organic solvent propylene glycol may stabilize the tetragonal $CdWO_4$, while (2) the presence of water in the reaction systems would favor the formation of the monoclinic. Therefore, getting rid of water from the reaction system is key for the selective preparation of single-phase tetragonal $CdWO_4$. However, such a task seems impossible when using starting materials $CdCl_2 \cdot 2.5H_2O$ and $Na_2WO_4 \cdot 2H_2O$, since the crystal water is very difficult to be completely removed from the starting materials. Here, we explored an alternative route to prepare the tetragonal $CdWO_4$ using an organic solvent of propylene glycol.

This alternative route was based on a two-step reaction. Namely, in the first step, starting materials $CdCl_2 \cdot 2.5H_2O$ and $Na_2WO_4 \cdot 2H_2O$ were dissolved in water separately to get their own aqueous solutions. Then, both solutions were mixed fully together, and a homogeneous precipitate was formed. To get rid of the water residual originated from the starting materials, the freshly prepared precipitate was sufficiently washed with anhydrous ethanol to obtain the precursor (XRD is given in Fig. 1d) for the second step to form the tetragonal $CdWO_4$. In the second step, the precursor was transferred to propylene glycol which was sealed in autoclave and allowed to react at 200 °C for 10 h. XRD pattern of the resulting product is shown in Fig. 1e. It is seen that the diffraction peaks for the monoclinic were hardly seen. All diffraction peaks are resembled with those for the typical scheelite compound $CaWO_4$ (JCPDS, No. 41-1431), although there exist systematic shifts in the diffraction peaks for both compounds. It can be thus concluded that tetragonal $CdWO_4$ was successfully prepared. In order to further exclude the effect from the crystal water, anhydrous metal salts were directly used as the starting materials with an aim to prepare tetragonal $CdWO_4$ in a propylene glycol-involved solvothermal process. However, under this condition, monoclinic phase of $CdWO_4$ was obtained along with some unknown phases (see Fig. 1f). It is interesting that tetragonal $CdWO_4$ was directly synthesized from solution chemistry, since tetragonal $CdWO_4$ is thermodynamically unstable (as supported by TG-DTA and XRD in Figs. S1 and S2) and can previously only be accessible under an extremely high pressure of 20 GPa [42]. Even so, when using the present methodology, the preparation of tetragonal $CdWO_4$ is highly reproducible.

3.2. Structure and morphology of both polymorphs

Crystal structure for the tetragonal $CdWO_4$ was optimized using Unitcell-97 program [46]. Initial atomic positions were adopted from a model tetragonal scheelite $CaWO_4$ ($I4_1/a$). The obtained lattice constants were $a=b=5.177$ Å and $c=11.132$ Å. These values are all smaller than those reported for $CaWO_4$ ($a=b=5.243$ Å and $c=11.374$ Å), which is apparently in accordance with the ionic size of Cd^{2+} smaller than Ca^{2+}. Additionally, oxygen atom positions were refined to 0.1539, 0.0066, and 0.2087. As a reference, the structural refinement of monoclinic $CdWO_4$ was also done and the corresponding lattice constants are $a=5.028$ Å, $b=5.864$ Å, $c=5.076$ Å, $\beta=91.53°$, and the atoms positions of two types of oxygen are at 0.2592, 0.3782, 0.3839, and 0.1800, 0.0879, −0.0661, respectively.

With the data of the structural parameters and atomic positions, the crystal structures for both polymorphs of the tetragonal and monoclinic were constructed. As displayed in Fig. 2, in the tetragonal structure of $CdWO_4$ (space group of $I4_1/a \equiv C_{4h}^6 \equiv$ no. 88, $Z=4$), tungsten ions are located in the centers of normal coordination tetrahedra, showing four W–O bonds with the same bond length of 1.758 Å. Just like many other scheelite-type compounds, the overall coordination number of Cd^{2+} is eight (Fig. 2a). These structural features are apparently different from those of the monoclinic (space group of $P2/c \equiv C_{2h}^4 \equiv$ no. 13, $Z=2$), where both W^{6+} and Cd^{2+} have octahedral oxygen coordination and each octahedron shares two corners with its neighbors (Fig. 2b). The WO_6 octahedra in the monoclinic are heavily distorted, with two of the W–O distances (1.806 Å × 2) being much shorter than those of other four (1.930 Å × 2, 2.218 Å × 2).

The structural order at short-range in both polymorphs was determined by measuring the Raman-active phonon modes. Group theory calculation predicts 26 vibration modes for the tetragonal primitive cell at wavevector $k=0$, which can be represented as follows [47]:

$$\Gamma = 3A_g + 5A_u + 5B_g + 3B_u + 5E_g + 5E_u \quad (1)$$

where all 13 vibrations A_g, B_g, and E_g are Raman-active. Comparatively, group theoretical analysis of the monoclinic yields 36 lattice modes at the Γ point [42]:

$$\Gamma = 8A_g + 10B_g + 8A_u + 10B_u \quad (2)$$

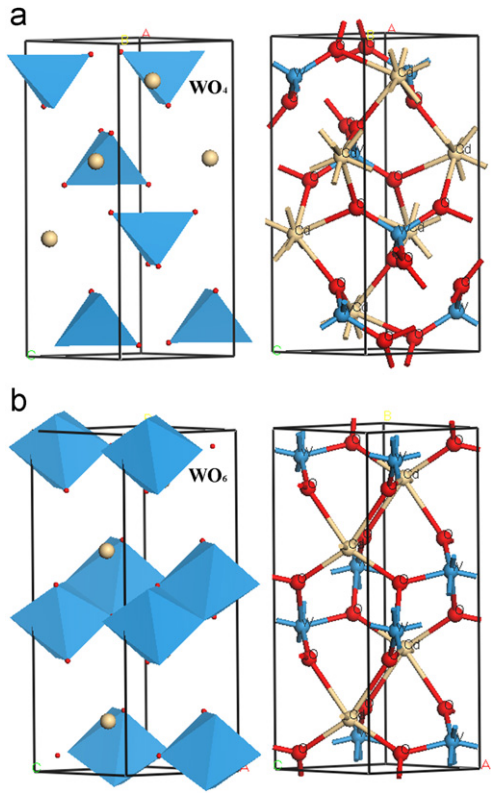

Fig. 2. Schematic polyhedron and ball-and-stick models for (a) tetragonal and (b) monoclinic $CdWO_4$.

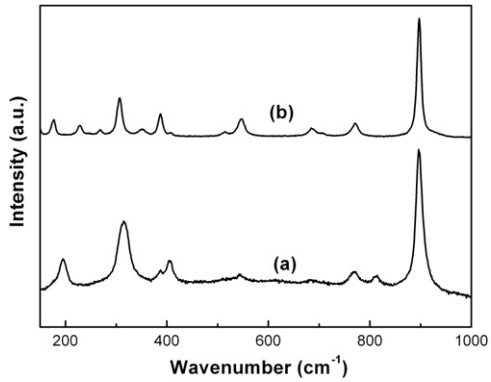

Fig. 3. Raman spectra for both polymorphs of (a) tetragonal and (b) monoclinic $CdWO_4$.

where 18 even (g) vibrations are Raman-active modes. Apparently, tetragonal $CdWO_4$ is predicted to have less Raman vibrations than the monoclinic $CdWO_4$ because of the increased lattice symmetry. Therefore, Raman spectroscopy is efficient to distinguish the phase structure of both polymorphs of $CdWO_4$. For the tetragonal, as indicated in Fig. 3a, there are three primary strong vibrations located at 897, 314, and 195 cm^{-1} and three weak vibrations at 814, 769, and 404 cm^{-1}. The most intense modes at 897 and 314 cm^{-1} and the weak mode at 769 cm^{-1} can be assigned to the W–O stretching vibration of WO_4 tetrahedra [43]. The medium mode at 195 cm^{-1} is derived from symmetric stretching vibration of the CdO_6 octahedra [42,43]. All these modes are characteristic of the tetragonal scheelite structure [43,48–50]. As for the monoclinic, the corresponding spectrum in Fig. 3b shows only one strong vibration at 896 cm^{-1} and several weak vibrations at 771, 687, 545, 515, 386, 348, 305, 269, 229, and 176 cm^{-1}. The vibration modes located at 896 and 386 cm^{-1} correspond to the normal W–O vibrations of the WO_6 octahedra, while the modes located at 771 and 687 cm^{-1} involve motions of WO_6 octahedra against the Cd^{2+} [42,51]. Bands in the range of 500–600 cm^{-1} are characteristic of symmetric W–O–W stretching modes [51]. The medium strong peak at 305 cm^{-1} is derived from the symmetric stretching of CdO_6 octahedra, and the other bands in the 300–150 cm^{-1} region can be assigned to the modes associated with Cd–O stretching [51]. Therefore, these comparative Raman studies further confirmed that tetragonal and monoclinic $CdWO_4$ were successfully selectively prepared.

Particle size and morphology of both polymorphs were examined using SEM. As indicated in Fig. 4, the tetragonal $CdWO_4$ exhibited a spherical morphology with an average size distributing in the range of 30–100 nm, whereas the monoclinic $CdWO_4$ exhibited a similar but more regular spherical morphology showing an average size of 50 nm. The BET measurements showed that the surface area for the tetragonal $CdWO_4$ was 19.03 m^2/g, which is slightly larger than that of 12.80 m^2/g for the monoclinic $CdWO_4$.

3.3. Electronic structures of both polymorphs

The electronic structures of both polymorphs were studied by experimental determination of the band-gap energy in combination with a theoretical calculation of the total densities of states. The band-gap energies for both polymorphs were determined by measuring the diffuse reflectance spectra (Fig. 5a). For a semiconductor, the optical absorption band-gap E_g was deduced according to:

$$(\alpha h\nu)^n = A(h\nu - E_g) \quad (3)$$

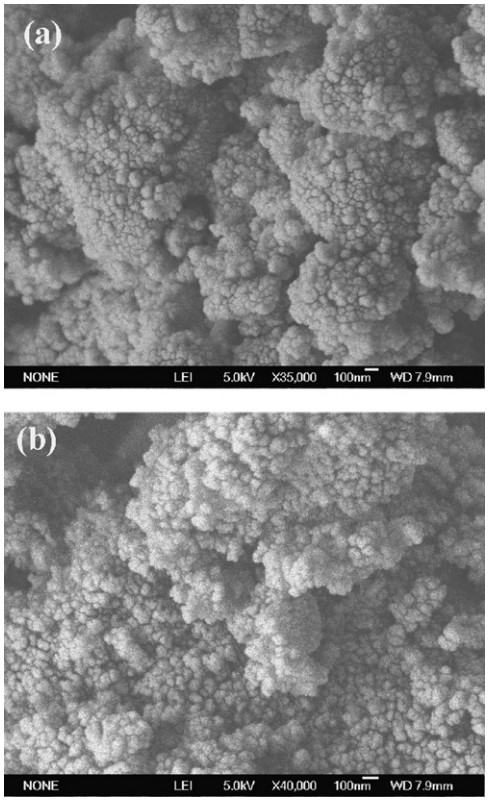

Fig. 4. SEM images for both polymorphs of (a) tetragonal and (b) monoclinic $CdWO_4$.

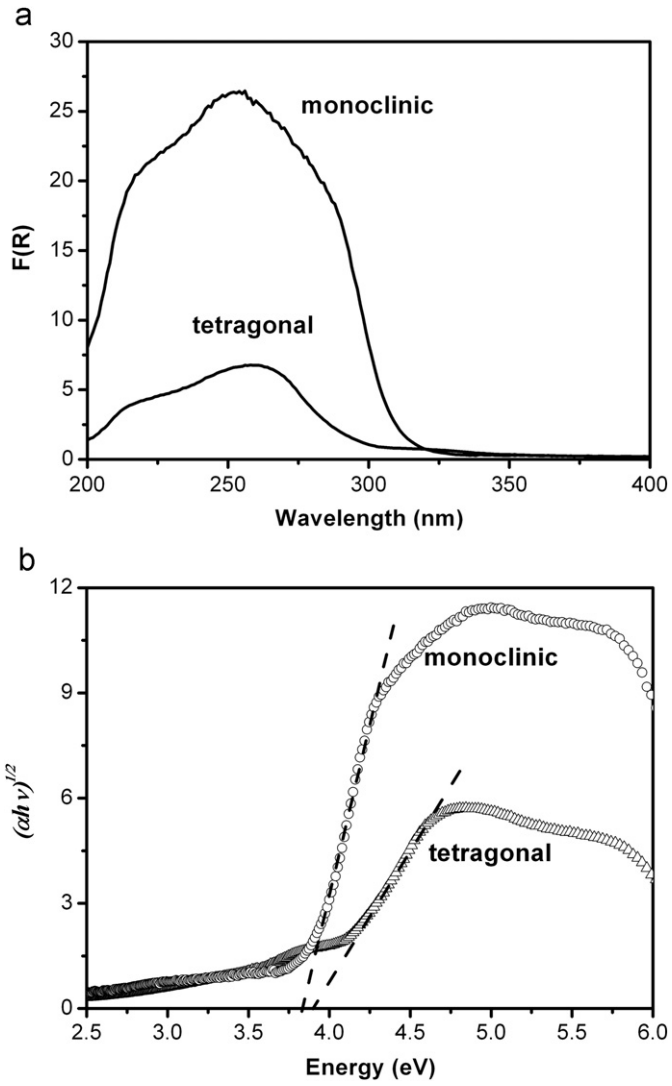

Fig. 5. (a) UV–vis diffuse reflectance spectra and (b) energy dependence of $(\alpha h\nu)^{1/2}$ for both polymorphs of monoclinic and tetragonal $CdWO_4$.

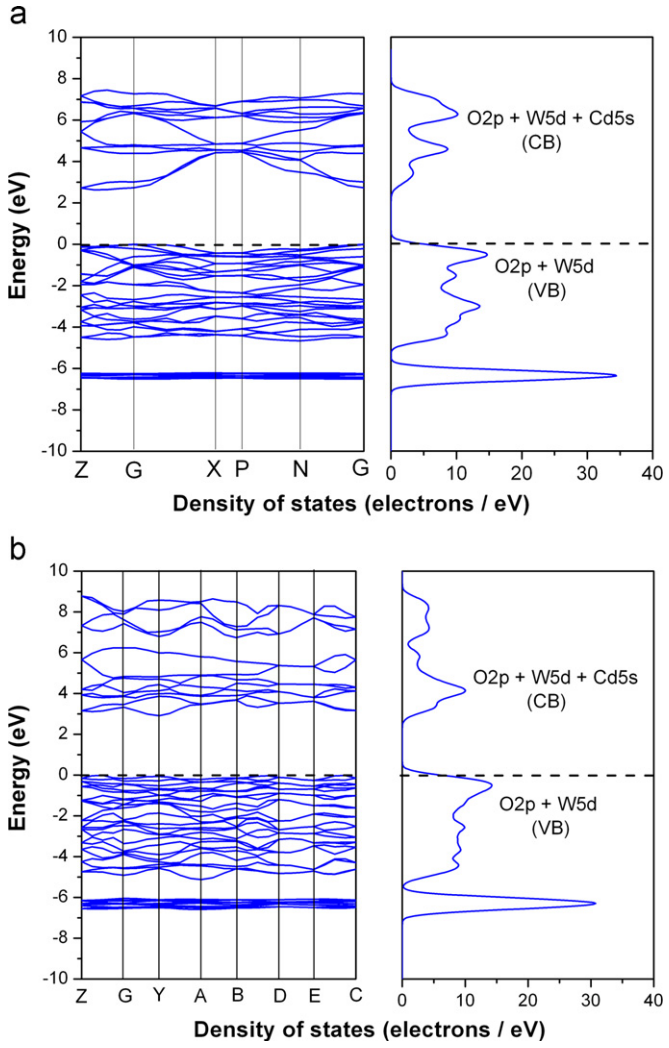

Fig. 6. Band structures and density of states (DOS) calculated for (a) the tetragonal and (b) the monoclinic polymorphs of $CdWO_4$ using density functional method.

where α is the absorption coefficient, $h\nu$ is the incident photo energy, A is a proportionality constant relative to the material, and E_g is the band-gap energy of the semiconductor. Depending on the types of electronic transition of a given semiconductor, the index n can be set as 2 for the direct transition or 1/2 for indirect transition. As for the present work, the calculated energy band structure in Fig. 6 revealed that the transition of both polymorphs was of indirect-type. Thus, the band-gap energy was obtained from the intercept of the straight line in the plot of $(\alpha h\nu)^{1/2}$ versus the energy (eV) (Fig. 5b). The estimated band-gap for the tetragonal was 3.90 eV, which is slightly larger than that of 3.83 eV for the monoclinic.

Since the tetragonal $CdWO_4$ is very difficult to be prepared, there is no report on its electronic structure. Here, the electronic structures of both tetragonal and monoclinic polymorphs of $CdWO_4$ were theoretically calculated using the plane-wave based DFT method, by taking into accounts the structural parameters determined above. Fig. 6 shows the band structures and total density of states (DOS) of both polymorphs. For the tetragonal, as shown in Fig. 6a, the valence band maximum (VBM) is located at the G point, while the conduction band minimum (CBM) is located near the middle point on the ZG line in the first Brillouin zones (BZ). Comparatively, for the monoclinic, the VBM and CBM is located near the middle point on the ZG lines in the first BZ and at Y point, respectively (Fig. 6b).

These results suggest that both polymorphs are semiconductors of indirect-type. The band-gap energies theoretically calculated for the tetragonal and monoclinic are 2.63 and 2.91 eV, respectively, which are both much smaller than those experimentally determined. The differences in band-gap energies may be originated from the discontinuity in the exchange-correlation potential that was not taken into account in the theoretical calculation. Similar to the previous report [34], the band structure calculation for the monoclinic $CdWO_4$ shows that the conduction band is dominated by O 2*p*, W 5*d*, and Cd 5*s* orbitals, while the valence band is mainly composed of the O 2*p* and W 5*d* orbitals (Fig. 6b). Quite similar to the monoclinic, the CB for the tetragonal $CdWO_4$ is consisted by O 2*p*, W 5*d*, and Cd 5*s* orbitals, and the VB by O 2*p* and W 5*d* orbitals. It is worthwhile to note that the CB width for both polymorphs is quite different: the CB for the tetragonal distributes from 2.45 to 7.45 eV (Fig. 6a), while for monoclinic $CdWO_4$, it ranges from 2.91 to 8.77 eV (Fig. 6b). The different electronic state distribution width in CB for both polymorphs is probably caused by the difference in their crystal fields around W atoms (tetrahedra vs octahedra). It is known that the crystal field can greatly influence the orbital distribution of the central atom [52]. In this sense, the tetragonal $CdWO_4$ contains WO_4 tetrahedra, while the monoclinic is consisted

of WO_6 octahedra. Due to the fact that the WO_6 crystal field is much stronger than WO_4, the former would result in a greater splitting of the W 5*d* orbitals and give rise to a wider W 5*d* electronic state distribution.

3.4. Photocatalytic activity comparison for both polymorphs

The distinct electronic structures for both polymorphs may give rise to different photocatalytic properties. The photocatalytic activities of both polymorphs were evaluated by degradation of MO in aqueous solutions under UV light irradiation of 254 nm. Prior to irradiation, the adsorption properties of these catalysts were initially studied. As shown in Fig. 7a, the adsorption/desorption equilibrium for both polymorphs was established after 40 min in dark and the adsorption amount for MO was so little and could be negligible. Temporal changes in MO concentration were monitored by examining the variations in maximal absorption in UV–vis spectra at 464 nm. Fig. 7b shows the temporal evolution of the spectral changes of the MO mediated by the tetragonal $CdWO_4$. It can be found that the concentration of MO decreases quickly under UV light irradiation with prolonging the irradiation time, and both absorptions at 464 and 270 nm characteristic of MO completely disappear after irradiation over the tetragonal $CdWO_4$ catalysts for 120 min. In contrast to tetragonal $CdWO_4$, as shown in Fig. 7a, the monoclinic $CdWO_4$ showed a higher activity in degradation MO: only an irradiation time of 80 min is needed for the monoclinic to completely degrade MO. For comparison, the photocatalytic activities of commercial TiO_2 (Degussa P25), $ZnWO_4$, and $CaWO_4$ were also tested under the same conditions. As illustrated in Fig.7a, all these catalysts have weak adsorption capacity towards MO and the photocatalytic activity is found to follow such a sequence, $TiO_2 >$ monoclinic $CdWO_4 \approx$ monoclinic $ZnWO_4 >$ tetragonal $CdWO_4 >$ tetragonal $CaWO_4$. We also tested the Cd^{2+} content of the residual solution after photocatalytic reactions. It is found that no Cd^{2+} was dissolved out from $CdWO_4$ when it was used as a photocatalyst, which indicates the high stability of $CdWO_4$ photocatalyst.

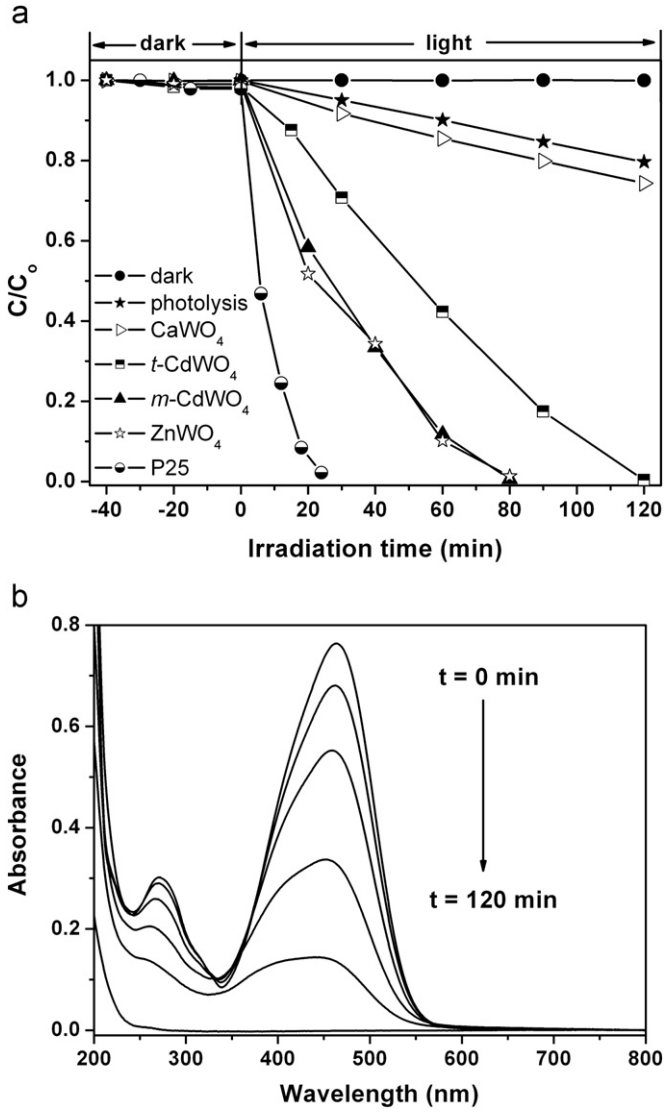

Fig. 7. Photocatalytic activities of both polymorphs (*t*-$CdWO_4$ and *m*-$CdWO_4$) for degradation of MO dye solutions under light irradiation of 254 nm: (a) concentration change profiles with irradiation time under different conditions and (b) absorbance variation of MO with irradiation time at the presence of the *t*-$CdWO_4$.

In order to clarify the effects of catalysis and photolysis, two control experiments were performed: one was performed in the dark with $CdWO_4$ catalysts, and the other was done under UV light irradiation without $CdWO_4$ catalysts. As shown in Fig. 7a, almost no MO degradation occurs in the dark. Instead, about 20% of MO can be directly decomposed by UV light irradiation. This observation cannot be ascribed to the dye-sensitization process as reported under visible light [53,54] where an electron is injected from dye molecules to the catalysts. This is because high energy of UV light is capable of directly destroying the chromophoric structure of dyes [55], while the visible light is not. Though MO is partially decomposed under UV light irradiation, the role of $CdWO_4$ is highly important since the surfaces of $CdWO_4$ under UV light irradiation may create abundant •OH radicals, which can be detected by a terephthalic acid (TA) photoluminescence probing technique [34]. Fig. 8a shows the photoluminescence (PL) spectra of tetragonal $CdWO_4$/TA solution under UV light irradiation. The result showed that the PL intensity of emission peak at 426 nm gradually increased with prolonging the irradiation time, indicating the generation of •OH radicals on $CdWO_4$ under UV light irradiation. From Fig. 8b, it can also be observed that the rate of •OH radicals generation over monoclinic $CdWO_4$ is higher than that over tetragonal, which is in accordance with their performance for MO degradation, suggesting that •OH radicals could be the main reactive species for MO degradation.

To understand the variation of photocatalytic activity of $CdWO_4$ polymorphs, several factors such as surface properties (e.g. surface charge, surface chemistry, and adsorption capacity), optical band-gap (i.e., optical absorption capability), surface area, separation/diffusion rate of the photogenerated charge carriers (mobility), and crystal structure should be addressed [2]. Among these factors, the surface property is considered as a most likely reason, since both $CdWO_4$ samples were obtained from different synthetic conditions. The chemical species absorbed on surfaces of $CdWO_4$ were examined by FT-IR spectra (Fig. S3). It is clear that only absorbed water and hydroxyl groups coexisted on the surfaces of both $CdWO_4$. The clean surface also implies that both $CdWO_4$ polymorphs have the similar surface charges. In addition, as stated above, both $CdWO_4$ samples have a similar adsorption capacity for MO. Therefore, the effect of surface property on photocatalytic activity of both $CdWO_4$ polymorphs can be ruled out in the present work.

With regards to the optical band-gap, it is well established that a wider band-gap may endow the photogenerated electrons and holes with stronger redox ability. In the present work, the effect of band-gap on the photocatalytic activity can be insignificant, since both $CdWO_4$ polymorphs had a similar band-gap (3.90 eV vs 3.83 eV). Many literatures reported that surface area of a given photocatalyst has a great influence on the photocatalytic activity [56,57]. For a catalyst with larger surface area, the ratio of the

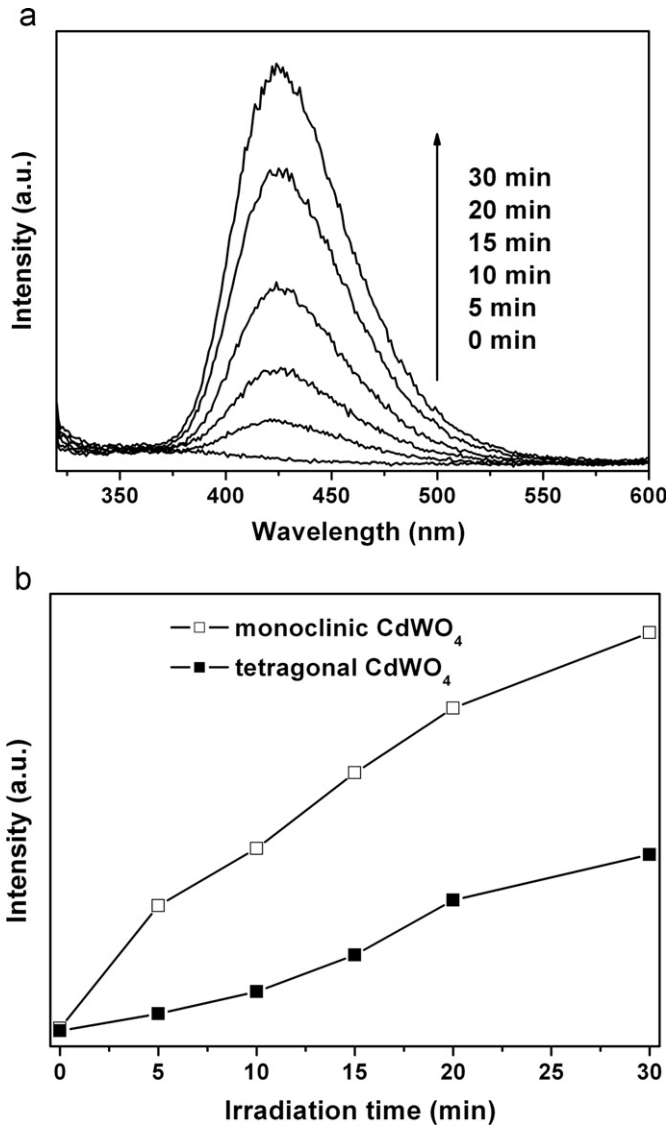

Fig. 8. (a) ●OH-trapping PL spectra of tetragonal $CdWO_4$/TA solution under UV light irradiation and (b) comparable plots of the induced PL intensity (at 426 nm) against irradiation time over both $CdWO_4$ polymorphs.

surface charge carrier transfer rate to the electron–hole recombination rate can be greatly improved, resulting in highly concentrated surface active sites and a higher photonic efficiency. However, larger surface area is usually associated with a large amount of crystalline defects or weak crystallization, which causes a poor photoactivity. Therefore, a large surface area is a requirement, but not a decisive factor. To reveal the intrinsic activities of the $CdWO_4$ polymorphs, we calculated the specific photocatalytic activity per surface area unit, for comparison, the data of TiO_2 (P25) was also given in Table S1. It is clear that monoclinic $CdWO_4$ exhibited the best specific photocatalytic activity, which is even higher than that of TiO_2. That means that surface area value is not responsible of the big difference in reactivity observed in Fig. 7a. On the basis of these considerations, there may exist other factors (rather than the band-gap and specific surface area) that might be responsible for the different photocatalytic activities of $CdWO_4$ polymorphs. One of the most likely factors is closely related to the polymorphs, which will be addressed firstly as below.

Based on the above-constructed crystal structures for both polymorphs of $CdWO_4$ (Fig. 2), it is apparent that the monoclinic $CdWO_4$ is constituted by distorted WO_6 octahedra, and their gravity centers heavily deviate from the W^{6+} position, which may generate dipole moments in the octahedral units. Comparatively, tetragonal $CdWO_4$ with much higher lattice symmetry contains only normal WO_4 tetrahedra, in which dipole moment could not be expected. There is a recent report [25] on the impacts of dipole moments on the photocatalytic activity for benzene degradation over three Ga_2O_3 polymorphs (α-, β-, γ-Ga_2O_3), in which crystal structure was found to play an important role in photocatalytic activity. Among three polymorphs, β-Ga_2O_3 with heavily distorted GaO_6 octahedra and GaO_4 tetrahedra is concluded to exhibit the best photocatalytic activity due to the existence of dipole moments in the tetrahedral and octahedral unit [25]. A good correlation between the photocatalytic activity for water splitting and the dipole moment has been demonstrated over some other wide-band-gap p-type semiconductor photocatalysts [58–60]. It is speculated that the existence of dipole moment in the distorted polyhedron would induce the local fields, which are positive for the efficient separation of excitons generated by light irradiation over the semiconductors. Therefore, a better photocatalytic activity for the monoclinic $CdWO_4$ than the tetragonal $CdWO_4$ observed in present work seems to be associated with their different geometric configuration and symmetry. Indeed, the different crystal structures for both polymorphs can also greatly influence their electronic structures, which could be the dominant factor responsible for the higher photocatalytic activity for the monoclinic.

One of the distinct features is *the electronic state distribution width of CB*. As indicated in Fig. 6, the electronic state distributions for both polymorphs are composed of hybridized orbitals of W 5*d* and Cd 5*s* as well as O 2*p* orbital, and therefore upon illumination, the excitons were generated, in which the electrons would transfer from O 2*p* to the hybridized orbitals of W 5*d* and Cd 5*s*. It is noted that the electronic state distribution width of CB for the monoclinic is greater than that for the tetragonal. The different width in CB distribution for both polymorphs is mainly caused by different crystal fields (tetrahedra and octahedra) around W atoms. In this case, monoclinic $CdWO_4$ contains WO_6 octahedra while tetragonal $CdWO_4$ is consisted of WO_4 tetrahedra. It is well documented that WO_6 crystal field is stronger than WO_4. The stronger crystal field would give rise to a greater splitting of the W 5*d* orbitals for a wider W 5*d* band distribution. Therefore, monoclinic $CdWO_4$ expects to have a greater CB distribution width, since its W 5*d* orbitals split greater than those in tetragonal. The greater electronic state distribution width represents a larger dispersion in *k*-space [61], which indicates that the photogenerated electrons in the monoclinic might possess smaller effective mass, just like what is reported for the charged particles tunneling through a crystal under an electronic filed [62]. Smaller effective mass for the monoclinic may give rise to larger migration ability, which is responsible for its high photocatalytic performance. Another distinct feature is *the band edge position in electronic structure*. The CBM observed for the monoclinic is about 0.46 eV higher than that for the tetragonal (Fig. 6). Therefore, photogenerated electrons in the monoclinic are expected to show higher energy, which would favor the high activity since interfacial electron transfer governs the rate of photocatalytic degradation of MO.

4. Conclusions

Tetragonal and monoclinic $CdWO_4$ were selectively prepared from an aqueous solvothermal process by adjusting the starting materials and solvents. It was shown that the tetragonal $CdWO_4$ could only be obtained in nearly anhydrous reaction conditions. The monoclinic $CdWO_4$ exhibited a much higher photocatalytic activity than the tetragonal $CdWO_4$ towards the degradation of MO dye solutions. Different from polymorphs (anatase, rutile, and

brookite) of the well-known photocatalytic material TiO_2 with the same building blocks TiO_6 octahedra, the present $CdWO_4$ polymorphs were constructed by distinct building blocks. Therefore, the findings reported in this work may provide useful information on the comprehension of the nature of the structure-sensitive photocatalytic activities that are highly necessary for developing new photocatalytic materials. Finally, it should be mentioned that both polymorphs of $CdWO_4$ have photo-absorption within the wavelength ranges shorter than that of TiO_2 because of the broad band-gap. Future work will examine methods of structural modifications for extending the photo-absorption to visible spectral region while maintaining the high photocatalytic activities.

Acknowledgments

This work was financially supported by NSFC (Nos. 50972143, 20831004, 21025104, 21025104), National Basic Research Program of China (2007CB613301), and Directional program CAS (KJCXZ-YWM10).

Appendix A. Supplementary material

Supplementary data associated with this article can be found in the online version at doi:10.1016/j.jssc.2010.12.013.

References

[1] M.R. Hoffmann, S.T. Martin, W. Choi, D.W. Bahnemann, Chem. Rev. 95 (1995) 69–96.
[2] A.L. Linsebigler, G.Q. Lu, J.T. Yates Jr, Chem. Rev. 95 (1995) 735–758.
[3] A. Fujishima, T.N. Rao, D.A. Tryk, J. Photochem. Photobiol. C 1 (2000) 1–21.
[4] Z.G. Zou, J.H. Ye, K. Sayama, H. Arakawa, Nature 414 (2001) 625–627.
[5] R. Asahi, T. Morikawa, T. Okwaki, K. Aoki, Y. Taga, Science 293 (2001) 269–271.
[6] T.L. Thompson, J.T. Yates Jr, Chem. Rev. 106 (2006) 4428–4453.
[7] X.C. Wang, K. Maeda, A. Thomas, K. Takanabe, G. Xin, K. Domen, M. Antonietti, Nat. Mater. 8 (2009) 76–80.
[8] H. Kominami, S.-Y. Murakami, J.-I. Kato, Y. Kera, B. Ohtani, J. Phys. Chem. B 106 (2002) 10501–10507.
[9] J.C. Yu, L.Z. Zhang, Z. Zheng, J.C. Zhao, Chem. Mater. 15 (2003) 2280–2286.
[10] C. Anderson, A.J. Bard, J. Phys. Chem. B 101 (1997) 2611–2616.
[11] K. Vinodgopal, P.V. Kamat, Environ. Sci. Technol. 29 (1995) 841–845.
[12] T. Takata, Y. Furumi, K. Shinohara, A. Tanaka, M. Hara, J.N. Kondo, K. Domen, Chem. Mater. 9 (1997) 1063–1064.
[13] H. Kato, A. Kudo, J. Phys. Chem. B 105 (2001) 4285–4292.
[14] J.H. Ye, Z.G. Zou, M. Oshikiri, A. Matsushita, M. Shimoda, M. Imai, T. Shishido, Chem. Phys. Lett. 356 (2001) 221–226.
[15] A. Kudo, K. Omori, H. Kato, J. Am. Chem. Soc. 121 (1999) 11459–11467.
[16] H. Kato, M. Hori, R. Konta, Y. Shimodaira, A. Kudo, Chem. Lett. 33 (2004) 1348–1349.
[17] L.Z. Zhang, I. Djerdi, M.H. Cao, M. Antonietti, M. Niederberger, Adv. Mater. 19 (2007) 2083–2086.
[18] L. Wang, W.Z. Wang, M. Shang, S.M. Sun, W.Z. Yin, J. Ren, J. Zhou, J. Mater. Chem. 20 (2010) 8405–8410.
[19] A. Kudo, S. Hijii, Chem. Lett. 28 (1999) 1103–1104.
[20] J.W. Tang, Z.G. Zou, J.H. Ye, Catal. Lett. 92 (2004) 53–56.
[21] G.L. Huang, C. Zhang, Y.F. Zhu, J. Alloys Compd. 432 (2007) 269–276.
[22] J.G. Yu, J.F. Xiong, B. Cheng, Y. Yu, J.B. Wang, J. Solid State Chem. 178 (2005) 1968–1972.
[23] J.G. Yu, H.G. Yu, H.T. Guo, M. Li, S. Mann, Small 4 (2008) 87–91.
[24] F. Amano, K. Nogami, B. Ohtani, J. Phys. Chem. C 113 (2009) 1536–1542.
[25] Y.D. Hou, L. Wu, X.C. Wang, Z.X. Ding, Z.H. Li, X.Z. Fu, J. Catal. 250 (2007) 12–18.
[26] J.W. Tang, J.H. Ye, J. Mater. Chem. 15 (2005) 4246–4251.
[27] S.X. Ouyang, Z.S. Li, Z. Ouyang, T. Yu, J.H. Ye, Z.G. Zou, J. Phys. Chem. C 112 (2008) 3134–3141.
[28] V.A. Pustovarov, A.L. Krymov, B. Shulgin, Rev. Sci. Instrum. 63 (1992) 3521–3522.
[29] C.D. Greskovich, D. Cusano, D.R. Hoffman, J. Am. Ceram. Soc. Bull. 71 (1992) 1120–1130.
[30] S.P. Burachas, F.A. Danevich, A.S. Georgadze, Nucl. Instrum. Methods Phys. Res. B 121 (1996) 404–407.
[31] D. Brown, R.H. Olsher, Y. Eisen, J.F. Rodriguez, Nucl. Instrum. Methods Phys. Res. A 373 (1996) 139–151.
[32] C.L. Melcher, R.A. Manente, J.S. Schweitzer, IEEE. Trans. Nucl. Sci. 36 (1989) 1188–1192.
[33] W.M. Tong, L.P. Li, W.B. Hu, T.J. Yan, G.S. Li, J. Phys. Chem. C 114 (2010) 1512–1519.
[34] D. Ye, D.Z. Li, W.J. Zhang, M. Sun, Y. Hu, Y.F. Zhang, X.Z. Fu, J. Phys. Chem. C 112 (2008) 17351–17356.
[35] Y.G. Wang, J.F. Ma, J.T. Tao, X.Y. Zhu, J. Zhou, Z.Q. Zhao, L.J. Xie, H. Tian, Mater. Sci. Eng. B 130 (2006) 277–281.
[36] K. Tanaka, D. Sonobe, Appl. Surf. Sci. 140 (1999) 138–143.
[37] K. Lennstrom, S.J. Limmer, G.Z. Cao, Thin Solid Films 434 (2003) 55–61.
[38] S.H. Yu, M. Antonietti, H. Coffen, M. Giersig, Angew. Chem. Int. Ed. 41 (2002) 2356–2360.
[39] Y.J. Xiong, Y. Xie, Z.Q. Li, X.X. Li, S.M. Gao, Chem. Eur. J. 10 (2004) 654–660.
[40] H.W. Liao, Y.F. Wang, X.M. Liu, Y.D. Li, Y.T. Qian, Chem. Mater. 12 (2000) 2819–2821.
[41] Y.G. Wang, J.F. Ma, J.T. Tao, X.Y. Zhu, J. Zhou, Z.Q. Zhao, L.J. Xie, H. Tian, J. Am. Ceram. Soc. 89 (2006) 2980–2982.
[42] R. Lacomba-Perales, D. Errandonea, D. Martinez-Garcia, R. Hernández, S. Radescu, A. Mujica, A. Muñoz, J.C. Chervin, A. Polian, Phys. Rev. B 79 (2009) 094105–094115.
[43] A.J. Rondinone, M. Pawel, D. Travaglini, S. Mahurin, S. Dai, J. Colloid Interface Sci. 306 (2007) 281–284.
[44] M.D. Segall, P.J.D. Lindan, M.J. Probert, C.J. Pickard, P.J. Hasnip, S.J. Clark, M.C. Payne, J. Phys.: Condens. Matter 14 (2002) 2717–2744.
[45] D. Chen, G.Z. Shen, K.B. Tang, H.G. Zheng, Y.T. Qian, Mater. Res. Bull. 38 (2003) 1783–1789.
[46] T.J.B. Holland, S.A.T. Redfern, Miner. Mag. 61 (1997) 65–77.
[47] T.T. Basiev, A.A. Sobol, Y.K. Voronko, P.G. Zverev, Opt. Mater. 15 (2000) 205–216.
[48] A. Jayaraman, S.Y. Wang, S.K. Sharma, Phys. Rev. B 52 (1995) 9886–9889.
[49] G. Blasse, Inorg. J. Nucl. Chem. 37 (1975) 97–99.
[50] R.L. Frost, L. Duong, M. Weier, Spectrochim. Acta Part. A. Mol. Biomol. Spectrosc. 60 (2004) 1853–1859.
[51] M. Daturi, G. Busca, M.M. Borel, A. Leclaire, P. Piaggio, J. Phys. Chem. B 101 (1997) 4358–4369.
[52] M. Oshikiri, M. Boero, J.H. Ye, Z.G. Zou, G. Kido, J. Chem. Phys. 117 (2002) 7313–7318.
[53] X.L. Yan, T. Ohno, K. Nishijima, R. Abe, B. Ohtani, Chem. Phys. Lett. 429 (2006) 606–610.
[54] B. Ohtani, Chem. Lett. 37 (2008) 216–229.
[55] M. Muruganandham, M. Swaminathan, Dyes Pigm. 62 (2004) 269–275.
[56] Y. Ohko, A. Fujishima, K. Hashimoto, J. Phys. Chem. B 102 (1998) 1724–1729.
[57] D.E. Gu, Y. Lu, B.C. Yang, Y.D. Hu, Chem. Commun. (2008) 2453–2455.
[58] J. Sato, H. Kobayashi, K. Ikarashi, N. Saito, H. Nishiyama, Y. Inoue, J. Phys. Chem. B 108 (2004) 4369–4375.
[59] J. Sato, N. Saito, H. Nishiyama, Y. Inoue, J. Photochem. Photobiol. A Chem. 148 (2002) 85–89.
[60] J. Sato, H. Nishiyama, N. Saito, H. Nishiyama, Y. Inoue, J. Photochem. Photobiol. A Chem. 158 (2003) 139–144.
[61] K. Ikarashi, J. Sato, H. Kobayashi, N. Saito, H. Nishiyama, Y. Inoue, J. Phys. Chem. B 106 (2002) 9048–9053.
[62] V.I. Sugakov, S.A. Yatskevi, Phys. Status Solidi (b) 173 (1992) 601–606.